NASA CR-132548

SHEAR BUCKLING OF SQUARE PERFORATED PLATES

by John F. Grosskurth, Jr., Richard N. White,
Richard H. Gallagher, and Gareth R. Thomas

(NASA-CR-132548) SHEAR BUCKLING OF SQUARE PERFORATED PLATES (Cornell Univ.) 47 p HC $3.75 CSCL 20K

N75-12364

Unclas
G3/39 04300



Prepared under Grant No. NGL 33-010-070 by
CORNELL UNIVERSITY
Ithaca, NY 14850

for

NATIONAL AERONAUTICS AND SPACE ADMINISTRATION

ABSTRACT

The behavior of thin square perforated plates under the action of uniform shear deformation is studied experimentally and analytically using finite element analysis. Elastic Shear buckling strength is established as a function of the diameter of a round, centrally located hole in the plate. Post buckling behavior and the behavior of perforated plates with various ring stiffeners are also studied experimentally.

Key Words

Shear buckling

Plate buckling

Centrally located circular perforations in plates

Finite element analysis

Experimental study

Reinforcement

TABLE OF CONTENTS

	Page
List of Symbols	v
List of Figures	vii
List of Tables	viii
1. Introduction	1
2. Test Specimens and Experimental Program	4
3. Analysis	9
4. Results and Analysis - Test Comparisons	15
5. Concluding Remarks	21
References	23
Figures	24
Tables	42

PRECEDING PAGE BLANK NOT FILMED

LIST OF SYMBOLS

b	shorter side length of rectangular plate
d	diameter of hole
k	buckling coefficient
t	plate thickness
u	x direction displacement component
v	y direction displacement component
w	z direction displacement component
E	modulus of elasticity
$[K]$	linear stiffness matrix
N	unitless buckling parameter
$[N_1]$	geometric stiffness matrix
T	diagonal tension force
V	shear force
δ_{lat}	lateral displacement
λ	load intensity factor
ν	Poisson's ratio
σ	normal stress
τ	shear stress
Δ	nodal displacements
$\bar{\Delta}$	nodal displacements at unit load intensity

PRECEDING PAGE BLANK NOT FILMED

List of Figures

		Page
1.	Geometry of Test Specimen.	24
2.	Reinforcement Patterns Around Perforations in Plates with d/b = 0.4.	24
3.	Testing Apparatus.	25
4.	Exploded View of Test Fixture.	26
5.	Unperforated Test Specimen.	27
6.	Plate Element Nodes and Degrees-of-Freedom.	28
7.	Mode of Deformation of Specimen Due to Imposed Edge Displacements.	28
8.	Finite Element Gridworks.	29
9.	Finite Element Gridworks for Convergence Study of Shear Buckling Calculations for Unperforated Plate. (See Fig. 8a for 36-Element Gridwork).	30
10.	Comparison of Various Finite Element Models with Classical Solution.	30
11.	Comparison of Solutions for T_{cr} as a Function of d/b Ratio. Unstiffened Plates.	31
12.	Pre-buckling In-plane Stiffness as Function of Various d/b Ratios. Unstiffened Plates.	32
13.	Contour Plots of Normal Modal Displacements for Various d/b Ratios.	33
14.	T vs. δ_{lat} for Four Unstiffened Plates.	34
15.	Criteria for Defining Critical Buckling Load Applied to Test Data for Unperforated Plate.	35
16.	Buckling and Ultimate Loads Determined from Test Results for Various d/b Ratios.	36
17.	Post-buckling Behavior of Plate with Uniform Edge Shear Deformation with d/b = 0.6.	37
18.	Specimens after Testing.	38
19.	Comparison of Experimental and Analytical Buckling Loads for Various d/b Ratios.	39

PRECEDING PAGE BLANK NOT FILMED

20. T vs. δ_{lat} for Equal Cross-Section Stiffeners. 40

21. T vs. δ_{lat} for Equal Volume Stiffeners. 41

List of Tables

1. Comparison of Analysis and Test Strains at Selected Gage Locations. 42

2. Inflection Point Buckling Loads for Both Unperforated Plate and Stiffened and Unstiffened Plates with 4-Inch Perforation. 42

1. INTRODUCTION

Thin plates occur in a wide variety of structures. While a good deal of our early knowledge about the behavior of thin plates has evolved from research directed to civil engineering structures such as plate girders, new applications in aerospace structures and pressure vessels have accelerated research in recent years.

Whatever the application, plate elements often block access to some other portion of the parent structure. Perforations are made in plates to allow permanent passage of electrical, hydraulic, or other conduits, or simply to permit easy access for painting or servicing. Where a reduction in strength is permissible, a hole might be placed in a plate to reduce weight. This is common in aerospace structures. In some cases, the reduction in the strength of the plate can be offset by the presence of a stiffener.

Plate elements are often subjected to complex loading conditions. To understand the behavior of perforated plates under complex loads, we must first know something of their behavior under more simple loading conditions. The behavior of thin, square, perforated plates subjected to in-plane shear is studied experimentally and analytically in this report. The plates have clamped edges and centrally located, circular perforations. An experimental study of stiffened perforated plates is also presented here.

A key aspect in the behavior of any thin plate is its buckling strength. Thin plates commonly become unstable at stress levels far below the proportional limit of the material. In some cases, the large transverse deformations associated with buckling can be tolerated and only the ultimate strength of the plate is of any practical consequence. Elsewhere, aerodynamic or aesthetic considerations dictate that buckling cannot be allowed.

Plate buckling strength is usually expressed in terms of the critical stress, σ_{cr} or τ_{cr}. The critical stress is the stress which, when applied uniformly along the edges of the plate, produces instability. For an isotropic square plate of thickness t, width b, elastic modulus E, and Poisson's ratio ν, this stress can be expressed as

$$\sigma_{cr},\tau_{cr} = k \frac{\pi^2 Et^2}{12(1-\nu^2)b^2} \qquad (1)$$

where k is known as the stability coefficient. Stability coefficients for compression and shear buckling of plates with various aspect ratios and edge conditions have been calculated and can be found in Reference 1. For the case of shear buckling of a square plate with clamped edges, this coefficient has been determined by Budiansky and Connor (Ref. 2) to be 14.71.

Perforated plates, however, present some analytical problems. The case of the square perforated plate under edge compression has been studied quite extensively since 1947. The most important works in this period are those of Levy, et al. (Ref. 3), Schlac, (Ref. 4 and 5), Kawai and Ohtsubo (Ref. 6), and Vann and Vos (Ref. 7). The analytical methods used in these papers range from energy methods and numerical integration in the report of Levy, et al. to finite element analysis as used by Vann and Vos.

The above work excluded consideration of shear buckling. Infinitely long shear webs have received some attention, but their relevance to the square plate is minimal and they will not be discussed in this report. The first serious attempt at predicting the critical shear stress of square perforated plates was made by Kroll (Ref. 8) in 1949. Using Timoshenko's energy method, which calls for the evaluation of two double surface integrals, Kroll obtained theoretical buckling coefficients for simply supported square plates with circular holes having diameters (d) equal to 1/8 and 1/4 the length of a side.

Numerical integration was used, and 22 points were needed in each octant to reduce the error for the known unpierced case to less than 5%. Analysis of the perforated plates indicated that the smaller hole reduced the coefficient by only 0.2%, while the larger hole caused a 22.6% reduction in the coefficient. Hole reinforcements were also analyzed and were found to increase the coefficient by as much as 334% over that for an unreinforced hole.

In 1967, Rockey, Anderson, and Cheung (Ref. 9) solved the same problem using finite element analysis. With an idealization containing 56 triangular elements in the analyzed quadrant, the solution for the unperforated case differed from classical theory by 9.7%. Solutions for the perforated cases differed markedly from those obtained by Kroll.

Four hole sizes were analyzed with simply supported and clamped edges. For the simply supported plate with a hole diameter to plate width ratio d/b = 0.125, Rockey, et al. found a reduction in the buckling coefficient of about 15%, whereas Kroll reported only a 0.2% reduction. The two papers were in somewhat better agreement with respect to perforated plates with a hole diameter to plate width ratio d/b = 0.250, for which Rockey, et al. observed a 28% reduction in the buckling coefficient, compared to Kroll's 22.6%.

Rockey, et al, investigated hole reinforcements, like Kroll, and found them extremely effective in canceling losses in buckling strength due to perforations. An experimental program was conducted and agreement with their analysis was good for the smaller diameter holes. Agreement was not as good for the larger holes.

Both Kroll and Rockey, et al, studied uniform applied shear stress rather than the case encountered in testing, that of uniform shear deformation. This was most graphically apparent in the investigation of Rockey, et al., wherein uniform stress was analyzed and uniform deformation tested. While this distinction has little effect on the classical

case of the unperforated plate, it has definite consequences when a hole is introduced. As the diameter of the hole increases, the stiffness of the plate continues to change along the edge and the two cases become more dissimilar.

This distinction was observed for the perforated plate in compression by Schlack in 1964. It was taken into account in his analysis, which used the Rayleigh-Ritz energy method, and was borne out by his testing.

The study reported here is restricted to perforated plates subjected to uniform shear deformation. The choice of test specimen geometries and the experimental program are described in Section 2. An analytical approach to elastic stability of unstiffened perforated plates is presented in Section 3, along with a summary of computed results. The experimental results for both unstiffened and stiffened plates are given in Section 4 and comparisons between analysis and test results are made. The final section of the report contains the concluding remarks.

2. TEST SPECIMENS AND EXPERIMENTAL PROGRAM

Specimen Size and Materials:

The experimental program was conducted on 10" square aluminum plates with a thickness of 0.063". The 10" size was chosen for convenience. It was felt that plates of this size would be large enough for careful observation and instrumentation, and yet not too large to test in a standard testing machine. Larger plates would also have necessitated a larger and more costly test fixture.

The material and thickness of the plates were chosen to ensure elastic buckling. Since very thin plates would be difficult to handle and would probably have initial imperfections of more significance than thicker plates, the latter were considered more desirable than the former. Since buckling stress is proportional to the square of the

plate thickness and to the elastic modulus, thicker plates could only be used with lower modulus materials. Thus, aluminum, with an elastic modulus approximately one third that of steel, was chosen.

Using Eq. 1, it was found that aluminum plates with a thickness of 0.063" and a side length of 10" would have a critical stress of 5.4 ksi. This is well below the yield stress and proportional limit of most of the common structural aluminum alloys.

The specific alloy chosen was 6061-T6, which has a relatively high yield point, an extensive linear post-yield region in its stress-strain curve, and a relatively small difference between its yield stress and ultimate strength. Hence, it approaches the elastic-plastic properties of structural steel and was chosen on that basis.

Six tensile coupons were tested to evaluate the significant mechanical properties of the material. The properties of interest are the initial modulus of elasticity E, Poisson's ratio ν, the proportional limit σ_p, the yield stress σ_y, and the ultimate strength σ_u. The proportional limit was taken as the point at which tensile strain first deviated from linearity by 0.0001 and the 0.2% offset approach was used to define the yield point. The above properties, which did not vary significantly with the direction in which the material was rolled, were $E = 10.2 \times 10^6$ p.s.i., $\nu = 0.3$, $\sigma_p = 34{,}000$ p.s.i., $\sigma_y = 30{,}000$ p.s.i. and $\sigma_u = 45{,}000$ p.s.i.

Three groups of specimens were tested. The first group were simply unperforated plates, (Figure 1, d = 0), used to establish "benchmark" values for the buckling loads. The second group of specimens was used to study the influence of unstiffened hole size on shear buckling capacity. Central holes with diameters (d) of 2, 4, and 6 in. were cut in these specimens, giving perforated plates with d/b ratios of 0.2, 0.4, and 0.6.

The third group of specimens (Fig. 2) consisted of perforated plates with stiffening material added around the perforations for the purpose of increasing the buckling load up to or beyond the buckling load of the unperforated plates. Five stiffened plates with four-inch holes were tested. All five stiffeners were flat rings made of the same material as the basic plates.

Choice of Stiffeners

There are several rules encountered in practice which can be used to determine the size of the required stiffener. One such rule is to replace the cross sectional area of the hole with a stiffener of equal cross section. This notion would have a theoretical foundation if buckling were entirely an axial phenomenon, but since the flexural rigidity of the plate dictates the buckling load, this rule lacks proper theoretical justification.

Two approaches to the equal cross section rule were tested. Stiffener 1 was a 2" wide circular ring fastened to one side of the plate only, while stiffener 2 consisted of 1" wide circular rings fastened on both sides. Stiffener 1 used 20% more material than stiffener 2.

Another common criterion is to replace the volume of material removed by the hole with a stiffener of equal volume. This rule has no more theoretical justification than the first, but it does result in a plate made of the same amount of material as the unperforated plate.

Three different equal volume stiffeners were tested. Since all stiffeners were fabricated from material of the same thickness as the test plates, equal volume was equivalent to equal surface area. Stiffener 3 was a simple circular ring, similar to stiffener 1 but only 0.828" wide. Stiffeners 4 and 5 were fabricated from 5.012" squares to form square outer and circular inner boundaries.

Stiffener 4 was oriented with its edges parallel to those of the test plate, while stiffener 5 was oriented at 45 degrees. Since shear is not a radial phenomenon, there is no reason to believe that a circular ring is the most efficient use of available material. Moreover, square stiffeners are easier to fabricate than circular ones.

The reinforcing rings were attached to the plates with epoxy (Epon 907, produced by the Miller-Stephenson Chemical Company). In order to keep the thickness of the epoxy as uniform as possible, thin steel fibers (0.002" dia.) were placed between plate and stiffener at clamping points.

In each specimen, the epoxy was strong enough to hold the ring to the plate beyond the buckling load. However, the epoxy always failed in a brittle fashion shortly thereafter, making it impossible to evaluate ultimate loads.

Loading Apparatus and Test Procedures:

The fixture used for testing the plates was designed to simulate the action of uniform shear deformation for plates with clamped edges. Such ideal behavior required the somewhat complex fixture shown in Fig. 3. Specifically, the external edge members had to form a mechanism with hinges located at the four corners of the plate to allow the plate to distort from a square shape to a diamond shape as shear load was applied.

The desired loading and edge restraint was accomplished by using a frame that consisted of two separate pairs of frames. An exploded view of the system is shown in Figure 4, including a typical test specimen. The test specimen had a 3 in. wide strip along each edge to enable bolting of the specimen to the frame. The corners of the resulting 16 in. square plate were cut out, as shown in Figure 5, to eliminate any extraneous stresses that might arise from distortion of the areas outside the basic 10 in. dimension of the plate as shearing distortions were introduced in the specimen.

The inner pair of frames were intended to force the specimen edges to displace linearly. They were made of 3" x 3/4" steel, formed the 10" square boundary of the test plates and provided the clamped edges over a 3" strip around the perimeter of the plates. Attachment of the plates was made by a total of 52 1/2" diameter bolts arranged in two rows. The holes for these bolts had to be located with extreme accuracy to assure proper fit between the fixture and the specimens. Moreover, the bolts had to fit into the holes with a minimum of play so that the plate could bear on the bolts in the event that frictional forces were not sufficient to transfer load into the plate. It was expected that possible slippage at the frame-plate interface would not happen until after the plate had buckled.

The outer pair of frames, made of 2-1/2" x 1/2" steel, were connected to the inner pair through the central row of bolts. It was the outer pair that contained the corner pivots in the form of 1" diameter hardened steel pins. These pins also provided the diagonal load points.

The test set-up was assembled vertically in a deformation controlled testing machine capable of exerting a tension load up to 30,000 pounds.

The fittings on either end of the fixture were each fabricated from three separate pieces of steel so that they could easily be moved and assembled. With just one side of the fixture (inner and outer frames) assembled, the testing machine could be adjusted until the 52 connecting holes in the fixture and specimen lined up. The machine was kept in this position while assembly of the fixture was completed. There were no forces on the plate at this point and no further computations were necessary to determine the point of zero load.

The test specimens were instrumented with 1" gage length strain gages placed at points of local strain maxima to monitor in-plane behavior and check for local yielding.

In certain cases, strain gages were placed back-to-back on opposite faces of the test plates to aid in the detection of buckling. The points of maximum expected strain were determined from the computer analysis.

Dial gages were used to measure out-of-plane deflections. These gages were placed at locations of maximum transverse deflection, which were determined from the eigenvector obtained from the computer program. Strain and deflection gage readings were taken at small increments of tensile load. At each increment, the load was permitted to stabilize before the readings were taken. The results obtained and their interpretation in terms of buckling loads will be described in Section 4.

3. ANALYSIS

Formulation Basis

The analyses for initial buckling of the unperforated- and perforated-unstiffened plates were performed with use of a finite element computer program whose theoretical basis is described in References 11 and 12. We briefly outline in the following the key features of this theory and those factors which are relevant to the subject analyses.

The finite element used in this work is a triangular thin shell element, portrayed in Figure 6. The flat form of the element of course applies in the present work. The relationships for this element are constructed in the stiffness matrix format on the basis of a generalized potential energy approach. In accordance with this approach, an element stiffness matrix is first formed using rather simple displacement functions. These violate conditions of inter-element continuity of displacement when the element is joined to others of the same type. The continuity is "restored" by writing equations which stipulate the required continuity on each of the element boundaries. Such equations are constraint equations which are incorporated into the global analysis by means of the Lagrange multiplier method.

In this work the u, v and w displacement fields of the triangular element are chosen in the form of complete cubic polynomials. The vertex node points each have 9 degrees-of-freedom (the translational displacement and the first derivatives with respect to the normal coordinate, for each of the three translational displacement components), and a centroidal coordinate with the values of the three translational displacements as degrees-of-freedom. This formulation lacks interelement continuity of normal angular displacement across the element boundaries. This continuity is restored by writing a constraint equation which requires that the angular displacements at the midpoints of the sides of adjacent elements be equal.

The formulation for linear elastic instability analysis involves the formation of a linear stiffness matrix [K], and a "first-order" geometric stiffness matrix $[N_1]$. The geometric stiffness matrix is a function of the applied loads and is calculated on the basis of a reference value of such loads. The intensity of the applied loads to cause instability is λ times the reference value so that the value of the geometric stiffness matrix at buckling equals $\lambda[N_1]$. The condition for instability is that the determinant of the matrix $[K] + \lambda [N_1]$ equal zero, i.e.

$$|[K] + \lambda [N_1]| = 0 \qquad (2)$$

The computer program developed to implement the present element formulation seeks a zero determinant iteratively. Analysis is first performed for $\lambda = 0$ in order to establish a basis for computing $[N_1]$, using a reference value of the applied loads. λ is then set equal to 1.0 and the determinant is evaluated. These two points on the λ vs. determinant plot are sufficient to start a Lagrangian interpolation scheme for predicting a zero determinant. Thus linear interpolation is used first, followed by parabolic interpolation when three points are available, and so on until convergence is reached.

The curve of load versus determinant is convex, which is unusual in buckling phenomena. In a compressive buckling problem, the curve would be concave. The difference is that in the case of shear, the direction of the load is of no consequence, while if a compressive load were changed to tension, buckling would never take place. For shear buckling, the determinant iteration curve must be symmetric about the vertical axis and, hence, must be convex.

Finite Element Idealization

The inherent symmetry of the problem, illustrated in Figure 1. simplifies the analysis somewhat. With the axes oriented along the diagonals as shown, each quadrant is identical and only one need be analyzed. Care must be taken in the imposition of the proper boundary conditions along these axes. Along the x axis, for example, symmetry dictates that v and $\frac{\partial w}{\partial y}$ must both be zero. Since v is zero along the entire length of the axis, $\frac{\partial v}{\partial x}$ must also be zero. Finally, there can be no shear along the x axis. Since

$$\tau_{xy} = \frac{\partial v}{\partial x} + \frac{\partial u}{\partial y} \tag{3}$$

and $\frac{\partial v}{\partial x}$ has already been determined to equal zero, $\frac{\partial u}{\partial y}$ must also be zero. Four similar boundary conditions along the y axis can be determined.

An idealization using three intermediate radial lines dividing the plate edge into four equal lengths was used to simplify the introduction of various hole sizes. This is shown in Figure 8 for the four analytical models of this study, the unperforated plate and plates with three different hole diameters. In this way, the diameter could be changed from 0 to 0.6b by merely scaling coordinates and without changing the basic style of the grid.

The analysis was limited to holes no larger than 0.6b, in consequence of limits on the geometric form of individual finite elements. As triangular finite elements become elongated, their solution accuracy tends to deteriorate. For a

simple constant stress element, this effect becomes noticeable when the aspect ratio nears three but with the more sophisticated element used in this analysis this effect should not produce significant errors until the aspect ratio reaches five or six. The highest aspect ratio used in the present analysis was less than five. If a larger diameter hole were introduced, this difficulty would have to be dealt with and the basic style of the analysis grid would have to be changed.

Uniform shear deformation was applied as prescribed u and v displacements at each of the five edge nodes. This represents a departure from the case of uniform shear stress, wherein x and y forces would be applied to these five nodes. Some insight into the source of the prescribed displacements can be gained by referring to Figure 7, which shows that the edge "slides" along the axes, remaining straight, and without changing length.

For small deformations, the displacement of each point has the same component along the edge. Hence, 1-1' is equal to 5-5' and the u and v displacements of each point conform to the ratios listed below.

$u_1 = -1.0$	$v_1 = 0.0$
$u_2 = -0.75$	$v_2 = 0.25$
$u_3 = -0.50$	$v_3 = 0.50$
$u_4 = -0.25$	$v_4 = 0.75$
$u_5 = 0.0$	$v_5 = 1.0$

The nature of the eigenvalue iteration used in the computer program insures that these ratios do not change. Simulation of clamped supports along this edge was accomplished by suppression of w, $\frac{\partial w}{\partial x}$, and $\frac{\partial w}{\partial y}$ at each of the five nodes.

Convergence Study for Unperforated Plate

The first objective in the analysis was to determine the convergence properties of the solution. As in any finite element analysis problem, it is essential to establish that the results were converging to the correct solution as the grid was refined, and that the chosen grid refinement yields a sufficiently accurate answer.

The unperforated plate was used for this purpose. For an unperforated plate, uniform shear stress causes uniform shear deformation. Therefore, the two cases are identical, and the buckling load can be computed using Eq. 1.

Finite element solutions were obtained using gridworks of 12, 20, and 36-elements, respectively. The 12 and 20 element meshes are shown as Figures 9a and 9b, respectively. The 36 element mesh appeared as Figure 8a. The classical "exact" solution, from Ref. 1, is T_{cr} = 4,800 lb. The calculated results are T_{cr} = 5,226 lb., 5,114 lb., and 4,954 lb., from the gridworks at Figs. 9a, 9b, and 8a, respectively. The results, shown graphically in Figure 10, demonstrate that the numerical solutions are indeed converging to the classical solution. The 36 element mesh produces an answer which is only 3.2% high.

Perforated Plate Solutions

With sufficient convergence established, the buckling loads for the perforated plates could now be determined. The primary goal of these analyses was to establish the relationship between the buckling load and the hole diameter. To discuss these results, we must examine the manner of definition of critical loading.

In the case of applied uniform shear stress, it is perfectly reasonable to think in terms of critical shear stresses and buckling coefficients. There is a distinct value of shear stress which, when applied uniformly around the perimeter of the plate, causes instability.

When the plate is under the action of uniform shear deformation, shown in Figure 7, this is no longer the case. The shear stresses imposed by this deformation can be quite nonuniform. Moreover, they can be accompanied by direct stresses of the same order of magnitude. The critical stress concept is inappropriate under these conditions.

The critical displacement of one of the corners, or the critical rotation of an edge could accurately define the point of buckling, but neither of these values is of much interest to the design engineer. He is primarily concerned with the load which can be applied before the plate buckles. For this reason, the shear buckling strength will henceforth be expressed in terms of the critical diagonal tension force, T_{cr}. This will be defined as the total force which, when applied across either diagonal of a square plate which is constrained to uniform shear deformation, causes elastic instability.

The relationship between buckling strength and hole diameter is shown in Fig. 11. This curve, particularly in the region of small diameters, is approximately parallel to and in fairly close agreement with the findings of Rockey, et. al. (Ref. 9), for uniform shear stress which are also shown in Figure 11. Although the percentage discrepancy of the two solutions grows with d/b ratio, the absolute difference between them remains essentially constant. In assessing this error, it must be recognized that different types of elements and gridwork refinements are used in the two approaches and the associated finite element discretization error is likely to be on the order of the indicated discrepancy. Differences in the imposed boundary conditions might also play a role.

The properties of Fig. 11 can be given an intuitive interpretation. A small hole would not be expected to greatly reduce the flexural stiffness of the plate, but would rather increase the stresses by the factor (1 -d/b).

This is precisely what is observed. As the diameter increases, the reduction in plate stiffness becomes more significant, causing the curve to become concave.

The buckling load does not give all the pertinent data about the behavior of perforated plates. Also of interest is the in-plane stiffness, which can be thought of as the diagonal tension force per diagonal extension. Figure 12 shows that the prebuckling stiffness, defined as the ratio of the diagonal force T and the corresponding corner point displacement u, does not change much when a small hole is introduced, but decreases rapidly with increasing hole diameter. Hence, there is an inherent tradeoff involved in using plates with large perforations. Although the loss in buckling strength is less than proportional to the d/b ratio, the increased flexibility might make such a plate undesirable.

Further insight into the behavior of perforated plates can be gained through the examination of the buckling modes. The normal displacement contours for the four cases are shown in Figure 13. The oval nature of the buckling contours is readily verified by intuition. The region of negative deformation is, however, a bit more interesting. The fact that the area of negative deformation decreases in size as the hole diameter increases offers a clue to the region's behavior. It is a consequence of diagonal compression along the horizontal axis, which also decreases with increasing hole size. The unperforated plate deforms into three half-waves along the horizontal diagonal. When a hole is introduced, the interior edges are permitted to approach each other on the horizontal diagonal, reducing the buckling effect along the axis.

4. RESULTS AND ANALYSIS-TEST COMPARISONS

The test results on the perforated, unstiffened plates are presented in this section and compared with analytical values. This material is followed with a summary of the

experimental results for the stiffened perforated plates; no analytical results are available for the latter.

Perforated, Unstiffened Plates:

Buckling is a gradual process due to initial imperfections. These initial imperfections were more pronounced and the buckling loads more difficult to pinpoint in the plates with the larger holes. In all cases, buckling could be detected through the strain gage readings long before it could be discerned visually. Typical plots of load against transverse deflection are shown for the four plate configurations in Figure 14. These plots indicate the gradual nature of buckling in each case.

The problem of buckling point definition has been encountered before and various criteria have been established. For example, Rockey, et al. (9), defined th buckling load as the intersection of the projections of the straight portions of the load vs. lateral deflection plot. This method has little justification but does produce an answer which is near the center of the transition range. Figure 15a, a load vs. lateral deflection plot for the unperforated plate, shows that this criterion would indicate that the buckling load for this plate was 5,200 pounds.

Another criterion defines the buckling load as the inflection point on the load vs. lateral deflection curve. (See Fig. 15b). This point does have physical meaning. It is the point of minimum plate rigidity in that the curve has a steeper slope on either side of it. Buckling points defined in this way are on the upper end of the transition range. Figure 15b shows that the buckling load for the unperforated plate is 5,400 pounds when this criterion is used.

Strain gage data can also be used to define the buckling load. When two strain gages are placed back-to-back on opposite faces of a plate in a region where buckling produces curvature, the gages indicate equal strains until the curvature appears. The strain reversal criterion defines the

buckling load as the point at which the strains read from one of the gages change direction. Figure 15c, which represents strain gage data from the unperforated plate, indicates that this method would define the buckling load as 5,100 pounds. One difficulty met with the strain reversal criterion, is placement of strain gages. They should be placed at the point of initiation of buckling-induced curvature, but this point is not always known in advance.

Hence, the buckling load for the unperforated plate could be called 5,400, 5,200, or 5,100 pounds, depending on which criterion was used to define it. Although the inflection point method does not give the best answer for this case in terms of agreement with theory, it does have physical significance and always gives a well-defined point at the top of the transition region. For these reasons, the inflection point method is used to define the buckling point in this report.

The experimental versus analytical buckling loads for the four unstiffened plates were 5,400 lb. vs. 4,954 lb. for d/b = 0, 4,100 lb. vs. 3,940 lb. for d/b - 0.2, 2,700 lb. vs. 3,014 lb. for d/b - 0.4, and 2,200 lb. vs. 2,482 lb. for d/b = 0.6. Figure 16 shows this information graphically. In view of the difficulties encountered in defining experimental buckling loads, the results are in good agreement. The maximum deviation is about 10%.

The strains encountered prior to buckling do not agree quite as well with analysis. Table 1 compares strains from a selected gage in each test with the corresponding strain from the computer analysis. In each case, the comparison is made for a centrally located gage at about one half the buckling load of the plate. The maximum deviation in this comparison is 30%. This larger deviation than in other solution parameters (e.g. the critical structure) may be due to the presence of combined bending-flexure and the finite size of the gage, among other experimental effects. Also, in finite

element analysis with the displacement method, the strains are expected to be less accurate than the displacements, since they are given by the derivatives of the displacements.

Buckling was the phenomenon of primary interest throughout the testing program. However, post buckling behavior was also of interest, and each plate was tested to failure. Figure 17 shows, sequentially, the behavior of the plate with a six inch hole through the onset of buckling to ultimate load and failure. The vertical ridge which can be seen at the end of the sequence was typical for the perforated plates.

Figure 18 shows each test plate after being tested to its ultimate strength. Each perforated plate exhibited yielding in the direction of loading on either side of the hole. Eventually, the load decreased and fracture occurred at the same location. The unperforated plate yielded in bearing around the connecting bolts. Since this was an edge failure, it is difficult to draw conclusions on the ultimate strength of the unperforated plate.

Each perforated plate exhibited an ultimate strength equal to about four times its buckling capacity. The variation of ultimate strength with d/b ratio is shown in Figure 16.

In studies dealing with perforated plates under uniform shear stress, the relationship has been given as a plot of the buckling coefficient, k, against the d/b ratio. In this way, the results have been non-dimensionalized. In the present study, stresses are not constant and the buckling coefficient is not meaningful for reasons previously discussed. The following parameter has therefore been defined:

$$N = \frac{T_{cr}(1-\nu^2)b}{Et^3}$$

This dimensionless parameter is equivalent to $k\sqrt{2}\pi^2/12$ for the case of the unperforated plate.

The analytical results are plotted in this form in Figure 19. Also shown are the experimental results and the classical solution for the unperforated plate. In this figure, the measured thickness of each plate and the observed mechanical properties of the material were used in calculating each experimental point.

Using Figure 19, it is possible to evaluate the relative efficiencies of perforated and unperforated plates. It must be remembered that the introduction of a hole into a plate reduces both the buckling strength and the amount of material used. Consider, for example, a 100" square steel shear panel which must carry a diagonal tension load of 100,000 pounds. For an unperforated plate (d/b=0), the required thickness would be 0.257" and 2,570 cubic inches of material.

If the same shear panel were fabricated with a 50" diameter hole, d/b=0.5 and N = 9.4. Hence, the required thickness would be 0.318" and 2,560 cubic inches of material would be needed. This represents a slight saving over the unperforated plate. This is not a significant saving, although perforated plates would appear more efficient at smaller b/t ratios. However, other factors, such as stiffness, must be considered in the comparison. The in-plane stiffness of the perforated plate in the example would be much lower than that of the unperforated plate. Figure 12 indicates that the introduction of such a perforation would lower the stiffness by about 40% if it were not accompanied by a corresponding increase in thickness. Since the thickness increased by only 24% when the hole was introduced, the reduction in stiffness would be quite significant.

A similar reduction in the ultimate strength of the plate would be expected. Figure 16 indicates that the reduction in ultimate strength would be even greater than the reduction in stiffness, but exact evaluation of this reduction is not possible because of the edge failure encountered when testing the unperforated plate.

Moreover, initial imperfections are likely to be more serious in perforated plates. While diagonal tension tends to eliminate imperfections along the loaded diagonal of unperforated plates, this effect is not present in perforated plates, and perforated plates would also be more likely to have large imperfections in the first place. Although initial imperfections do not change the buckling load, they have severe effects on the plate behavior prior to buckling, causing large out-of-plane deformations.

Stiffened Perforated Plates

We consider now the experimental results for the stiffened perforated plates, (Figure 2), for which no analysis results are available. Figure 20 gives the load vs. lateral deflection (δ_{lat}) of the unstiffened plate to those of the same plate reinforced with stiffeners 1 and 2. Lateral deflections were measured at the expected point of maximum displacement. From this figure, it can be seen that both reinforcing schemes were quite effective in increasing the buckling loads of the perforated plates.

Evaluation of the buckling load for stiffener 2 was difficult, but no more so than it had been for the unstiffened plates. Due to the eccentricity produced by attaching a stiffener to only one side of the plate, however, the plate using stiffener 1 buckled quite gradually and determination of the inflection point involved a great deal of judgment. It must be noted that evaluation of the buckling loads for this and all other eccentrically stiffened plates carry with them an inherent judgment or uncertainty factor on the order of 15%.

Despite these difficulties, the inflection points were located and the buckling loads evaluated. It was found that stiffeners 1 and 2 increased the buckling loads by 237% and 318%, respectively, over the same perforated plate with no stiffener.

Figure 21 shows the load vs. lateral deflection curves for stiffeners 3, 4, and 5, along with a similar plot for the unstiffened plate. As this figure indicates, the shape and orientation of the stiffener made little difference in behavior. Each stiffened plate exhibited the same gradual buckling that was seen in the plate using stiffener 1. Each increased the buckling load by about 60% so that each stiffened plate had a buckling load approximately equal to that of an unperforated plate. Table 2 lists the inflection point buckling loads for all five stiffened plates as well as the buckling strengths of unstiffened plates with and without the 4" diameter hole.

Although the numbers found in this table indicate that the circular ring is the most efficient equal volume stiffener, the differences are too small to draw final conclusions. Indeed, if either strain reversal or the method of Ref. 9 had been used to define the buckling point, stiffener 5 would have appeared to be the most efficient, followed by stiffeners 3 and 4, respectively.

5. CONCLUDING REMARKS

The behavior of thin, square, perforated plates under the action of uniform shear deformation has been studied analytically and experimentally. The relationship between the elastic buckling strength and the diameter of a round, centrally located hole has been established using finite element analysis. Experimental results were in reasonable agreement with the analysis results.

The experimental program on stiffened plates indicated that a ring of the same material and thickness as the plate can be extremely effective in canceling the loss of buckling strength which accompanies the introduction of a perforation. Rings made of the same amount of material as the removed hole can increase the buckling strength back to that of an unperforated plate and, in this study, alternate reinforcing schemes increased the buckling load by as much as 318%.

Whereas buckling of unstiffened plates involves only one variable, stiffener design includes many, such as stiffener size, shape, location, or material type.

There is a considerable amount of additional research needed in the field of shear buckling of perforated plates. Problems that need attention include:

a. analytical treatment of stiffened plates, with particular emphasis on optimum stiffener geometry.

b. analytical and experimental study of plates with holes of differing shapes (such as rectangles) and at locations other than the center of the plate.

c. treatment of inelastic buckling and ultimate strength of plates.

Experimental studies of shear buckling are quite expensive and time consuming. They must be supplemented as much as possible with analytical approaches. It appears that finite element analysis capabilities could play a major role in any future research in plate buckling.

REFERENCES

1. Timoshenko, S. P., and J. M. Gere. Theory of Elastic Stability, Second Edition. McGraw-Hill, New York, 1961.

2. Budiansky, B., and R. W. Connor. Buckling Stresses of Clamped Rectangular Flat Plates in Shear. NACA Technical Note 1559, 1948.

3. Levy, S., R. M. Woolley, and W. D. Kroll. "Instability of Simply Supported Square Plate with Reinforced Circular Hole in Edge Compression", Research Paper RP1849, Journal of Research of the National Bureau of Standards, Vol. 39, 1947.

4. Schlack, A. L. "Elastic Stability of Pierced Square Plates", Experimental Mechanics, Vol. 4, No. 6, June, 1964.

5. Schlack, A. L. "Experimental Critical Loads for Perforated Square Plates", Experimental Mechanics, Vol. 8, No. 2, February, 1968.

6. Kawai, T., and H. Ohtsubo. "A Method of Solution for the Complicated Buckling Problems of Elastic Plates with Combined Use of Rayleigh-Ritz's Procedure in the Finite Element Method", Proceedings of the Second Air Force Conference on Matrix Methods in Structural Mechanics, October, 1968, pp. 967-994.

7. Vann, W. P., and R. G. Vos., Compressive Buckling of Pierced Elastic Plates. Structural Research at Rice, Report No. 14, Department of Civil Engineering, Rice University, Houston, Texas, August, 1972.

8. Kroll, W. D. "Instability in Shear of Simply Supported Square Plates with Reinforced Hole", Research Paper RP 2037, Journal of Research of the National Bureau of Standards, Vol. 43, November, 1949.

9. Rockey, K. C., R. G. Anderson, and Y. K. Cheung. "The Behavior of Square Shear Webs Having a Circular Hole" in Thin Walled Steel Structures, K. C. Rockey and H. V. Hill, Ed., Gordon and Breach, London, 1968, pp. 48-172.

10. Thomas, G. R. Finite Element Non-Linear Analysis of Shells. Ph.D. Thesis, Cornell University, August 1973.

11. Thomas, G. R. and R. H. Gallagher. A Triangular Thin Shell Finite Element: Linear Analysis. NASA CR (To be published).

12. Thomas, G. R. and R. H. Gallagher. A Triangular Thin Shell Finite Element: Nonlinear Analysis. NASA CR (To be published).

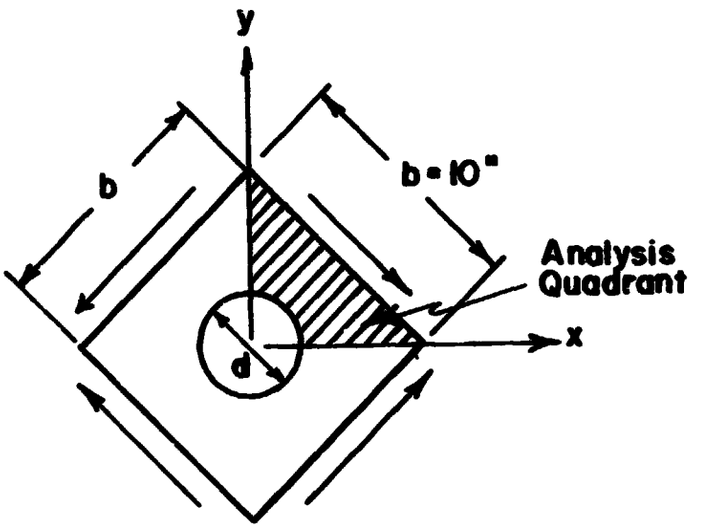


FIGURE 1 - Geometry of Test Specimens.

Stiffener	Geometry	c, in	Vol. Stiffener / Vol. Removed Material
1		2	3.00
2		1	2.50
3		0.828	1.00
4		0.506	1.00
5		0.506	1.00

FIGURE 2 - Reinforcement Patterns Around Perforations in Plates with d/b = 0.4.

REPRODUCIBILITY OF THE ORIGINAL PAGE IS POOR.

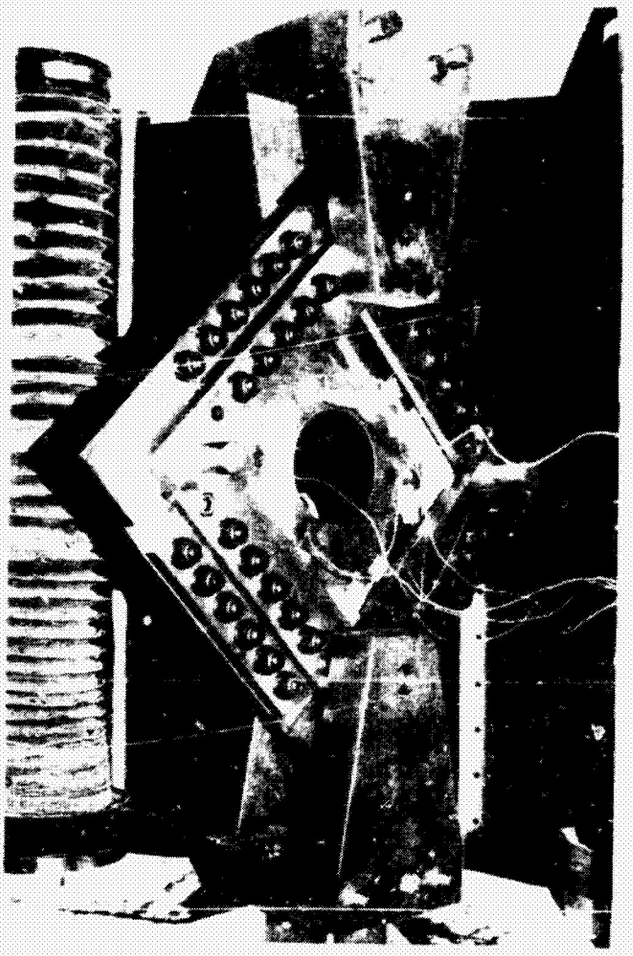


FIGURE 3 - Testing Apparatus.

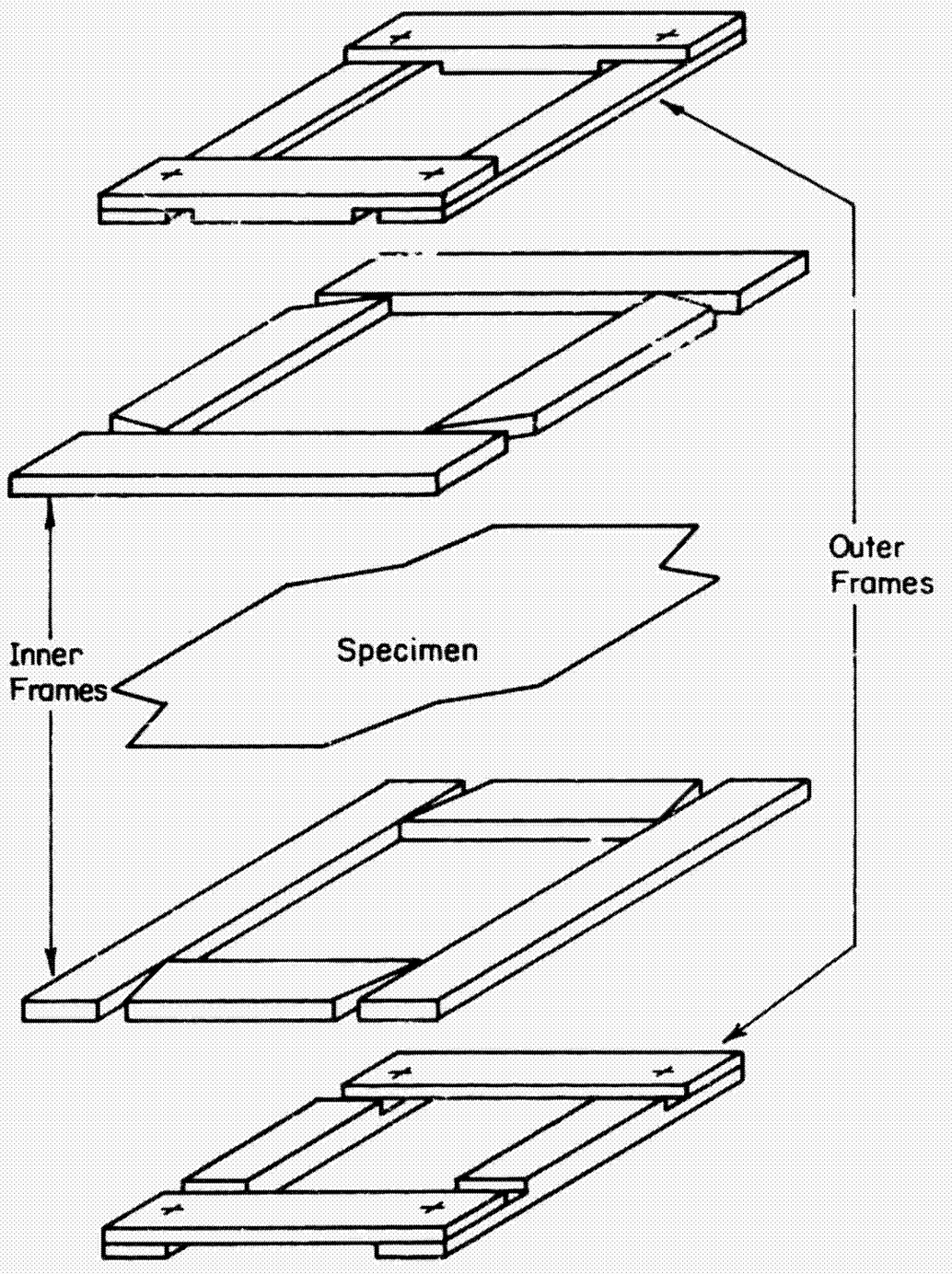


FIGURE 4 - Exploded View of Test Fixture

REPRODUCIBILITY OF THE ORIGINAL PAGE IS POOR.

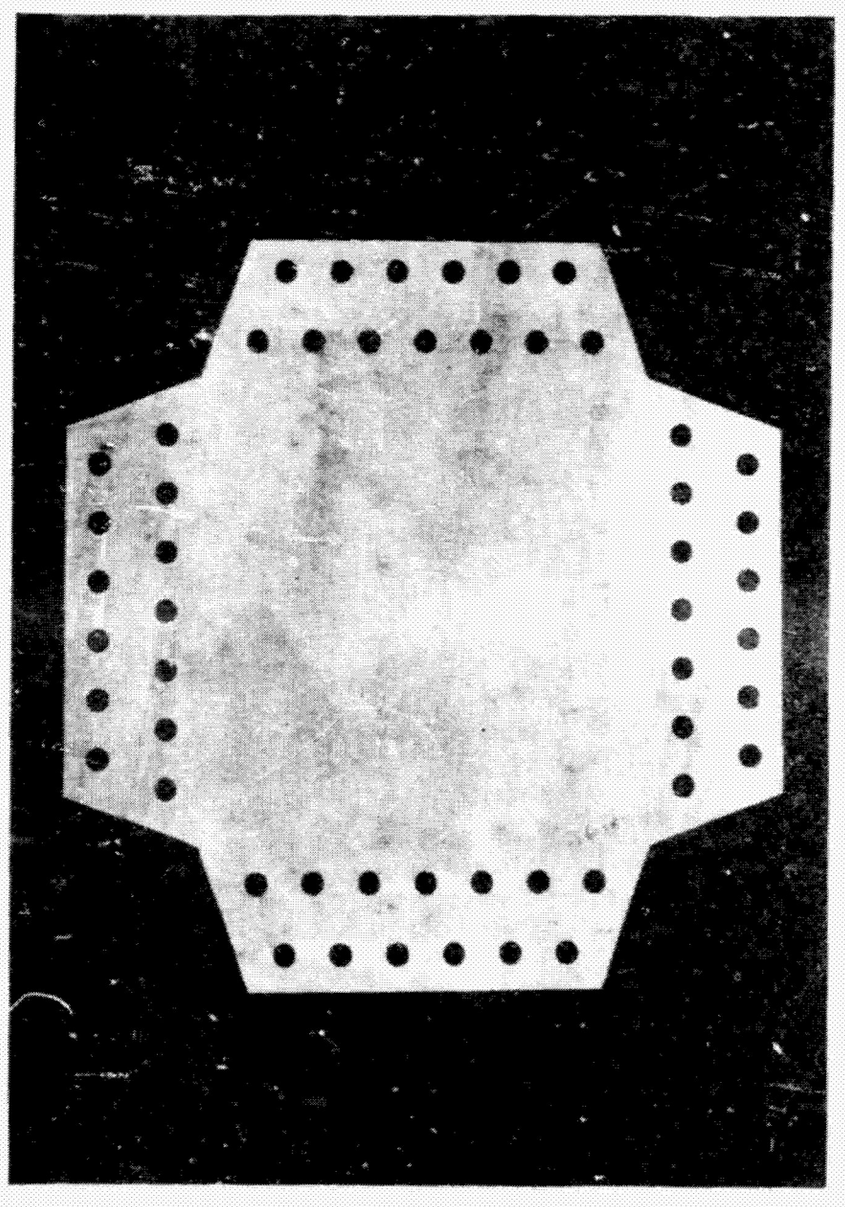


FIGURE 5 - Unperforated Test Specimen.

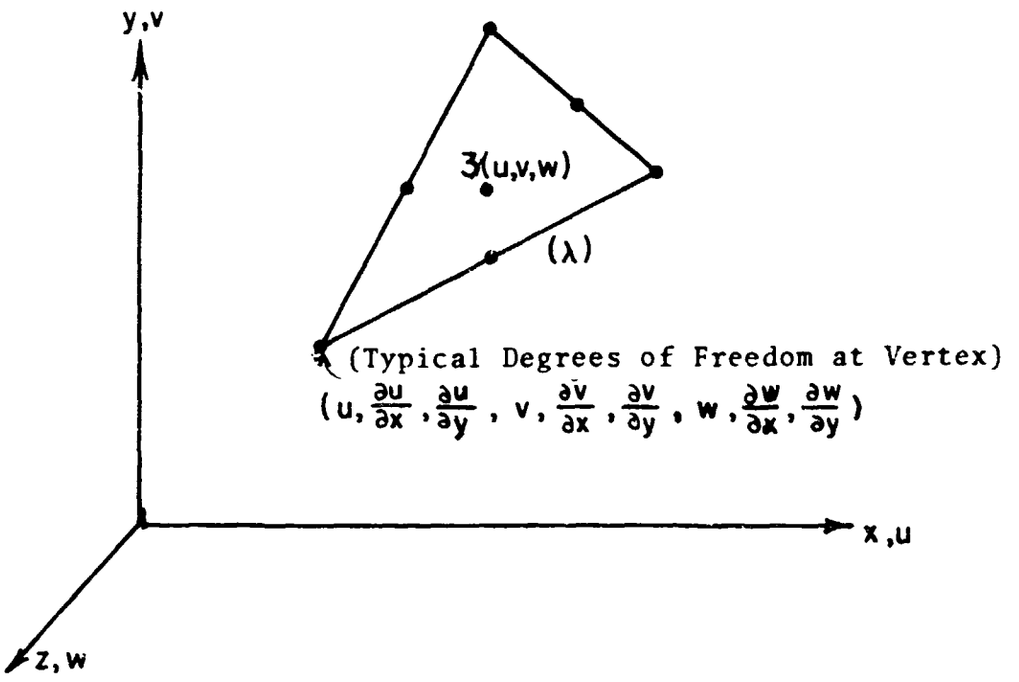


FIGURE 6 - Plate Element Nodes and Degrees-of-Freedom

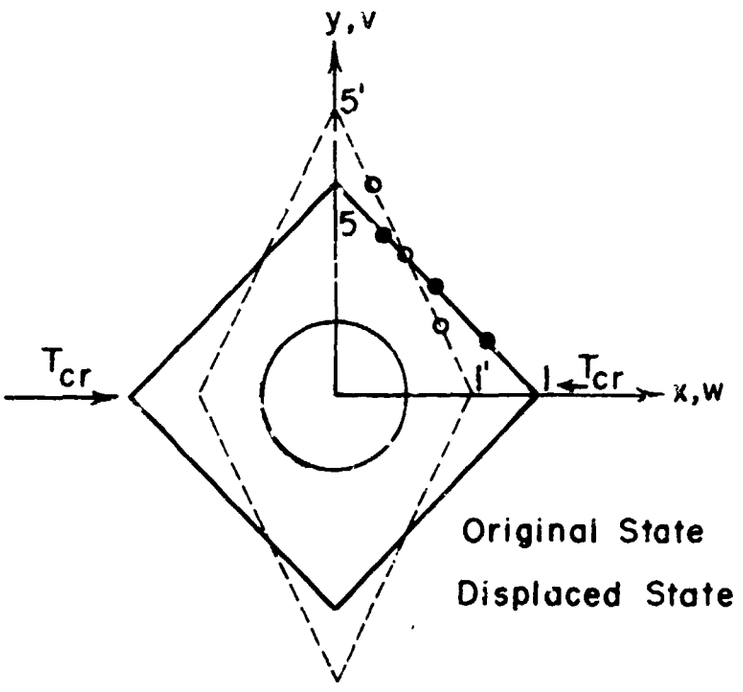
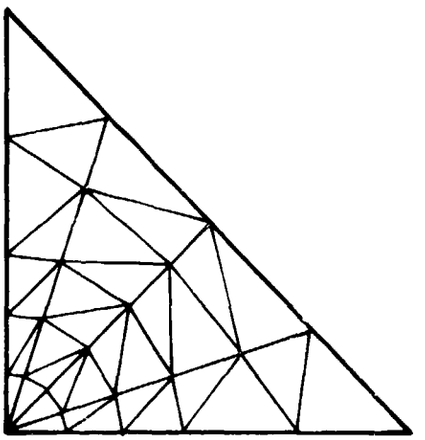
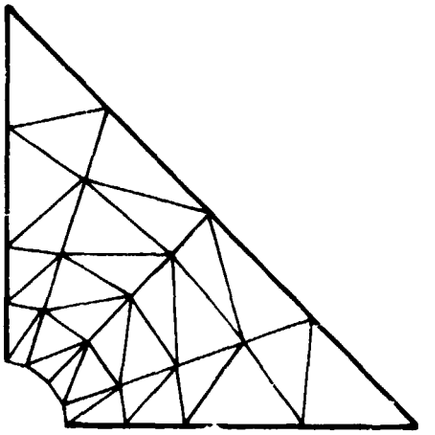


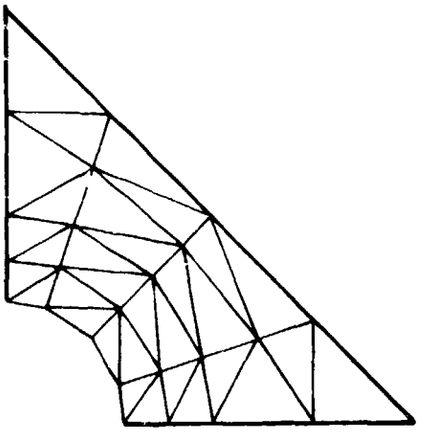
FIGURE 7 - Mode of Deformation of Specimen Due to Imposed Edge Displacements.



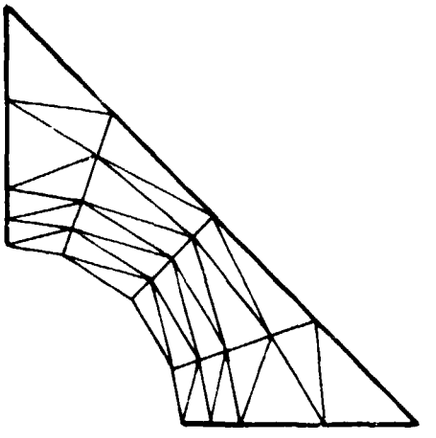
a. Unperforated



b d/b = 0.2



c. d/b = 0.4



d. d/b = 0.6

FIGURE 8 - Finite Element Gridworks

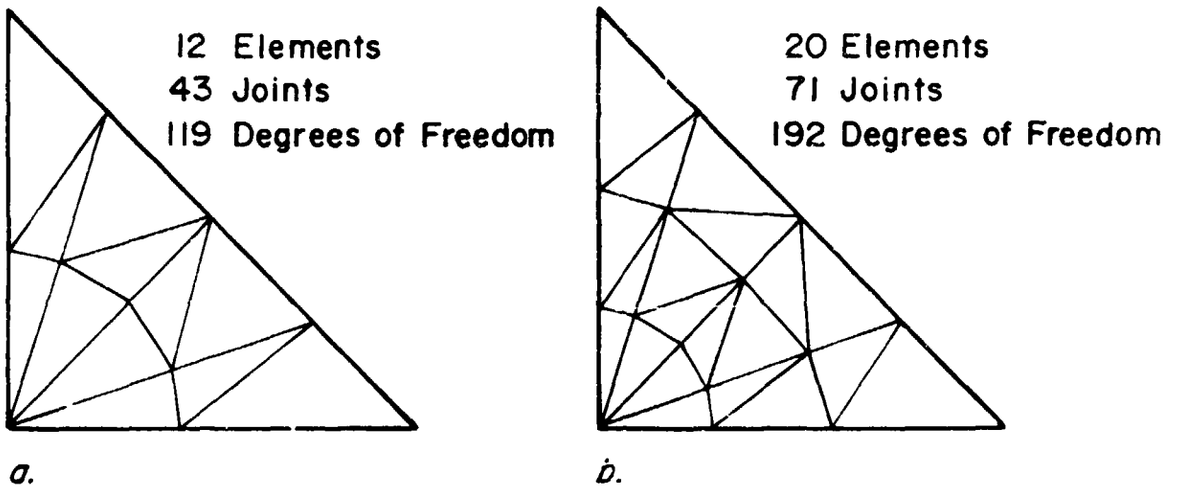


FIGURE 9 - Finite Element Gridworks for Convergence Study of Shear Buckling Calculations for Unperforated Plate. (See Fig. 8a for 36-Element Gridwork).

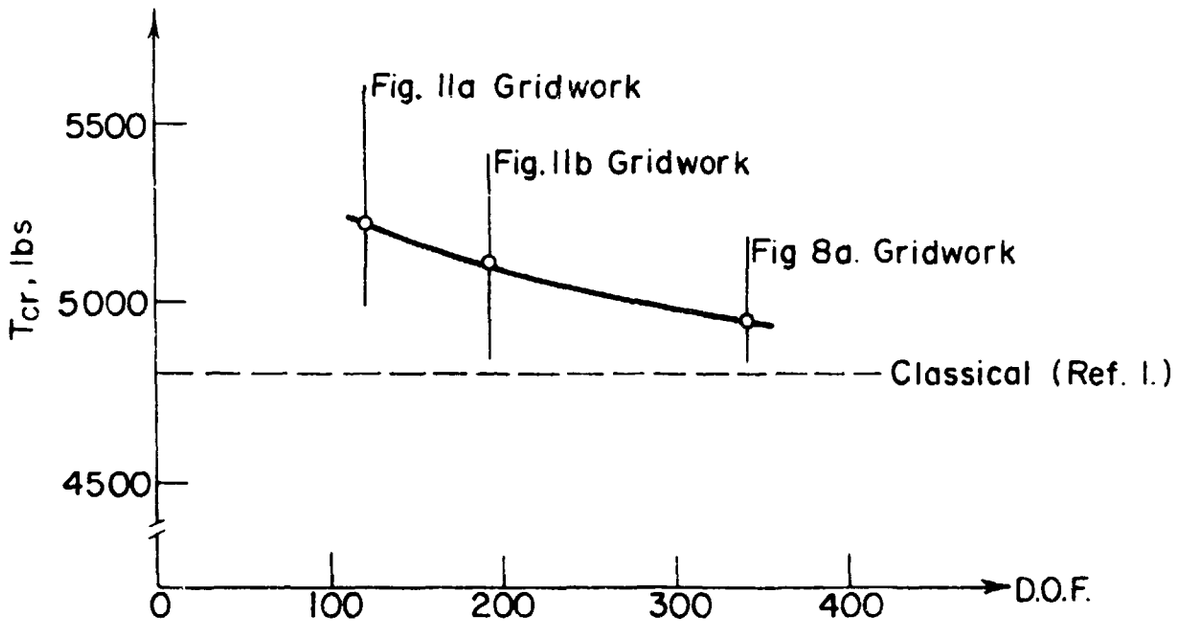


FIGURE 10 - Comparison of Various Finite Element Models with Classical Solution.

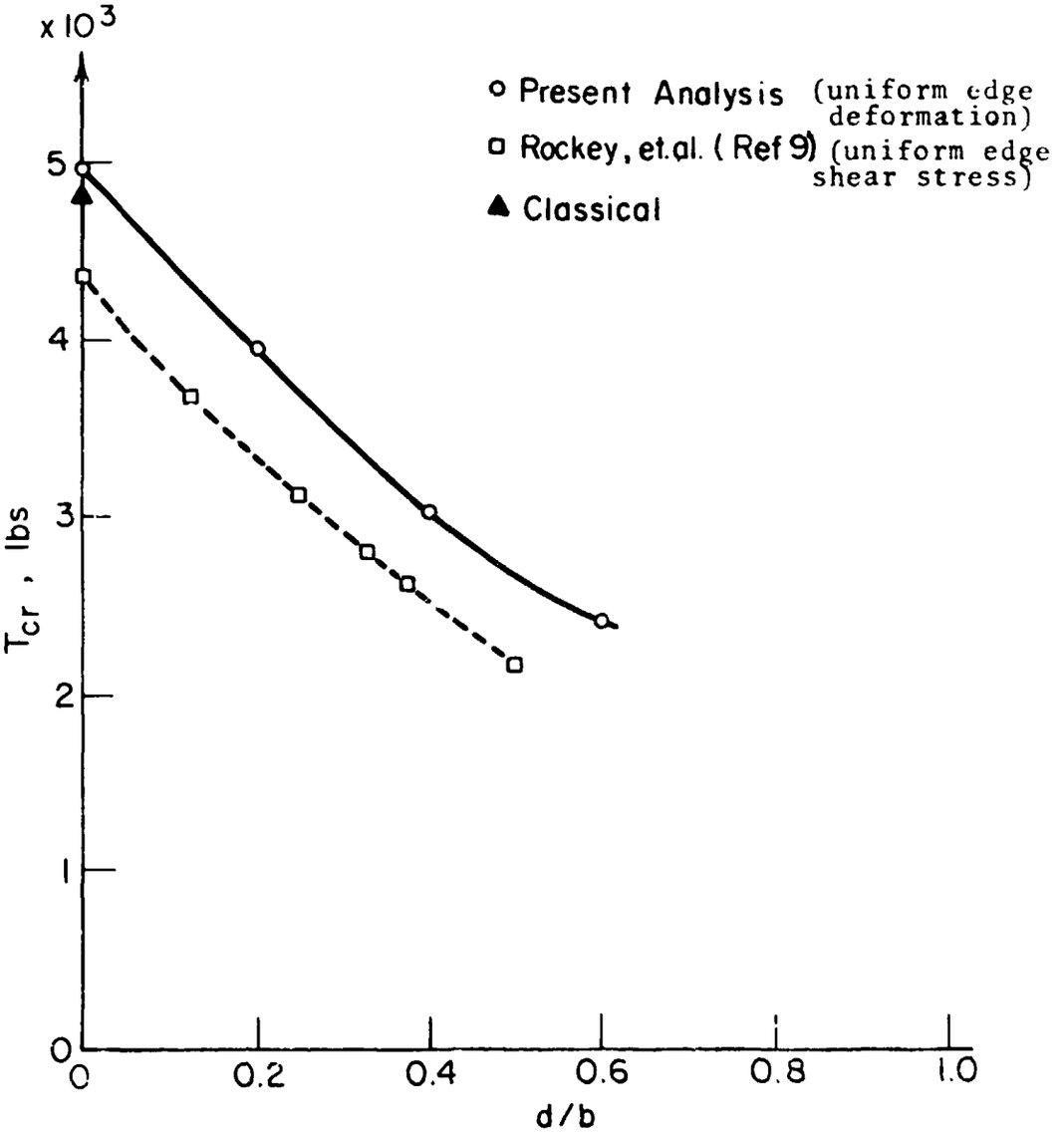


FIGURE 11 - Comparison of Solutions for T_{cr} as a Function of d/b Ratio. Unstiffened Plates.

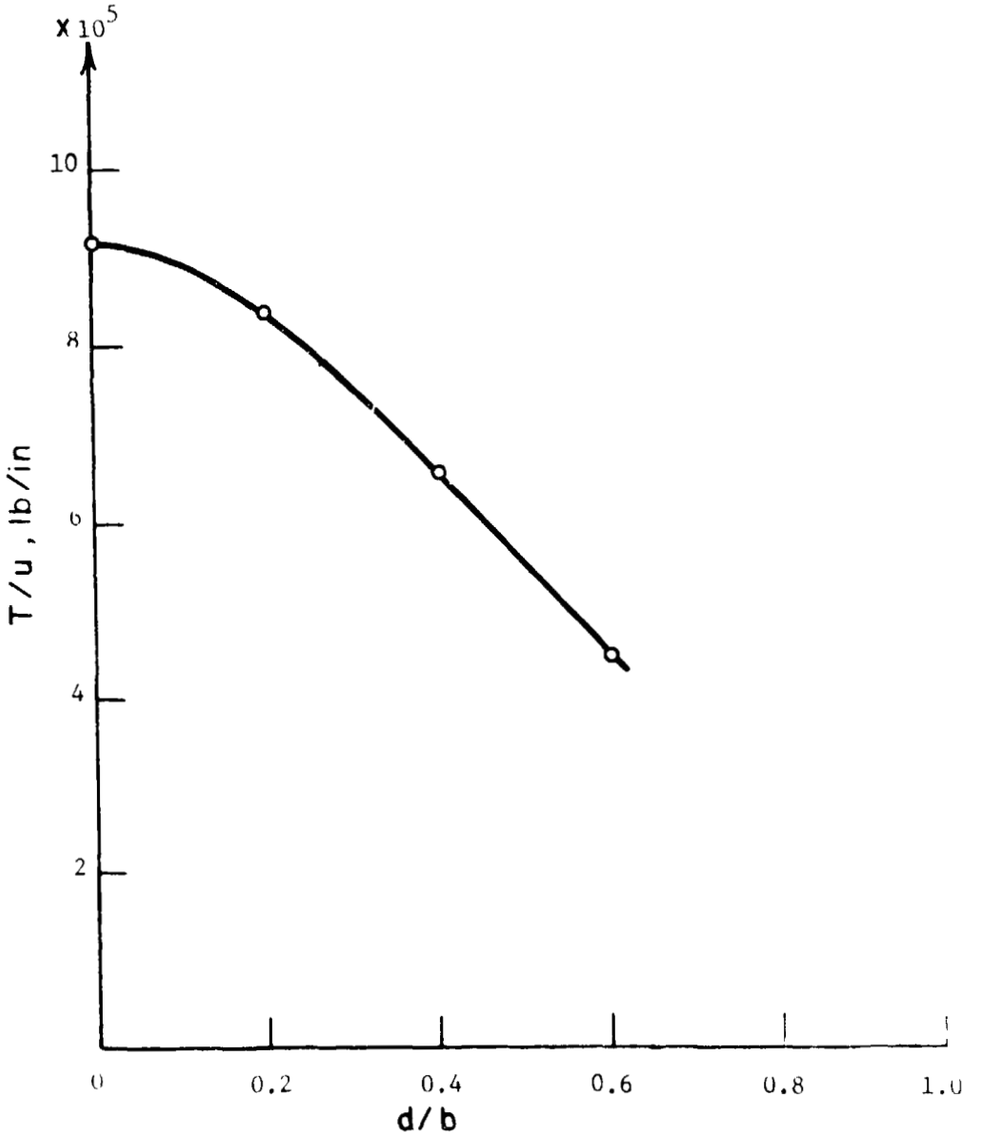
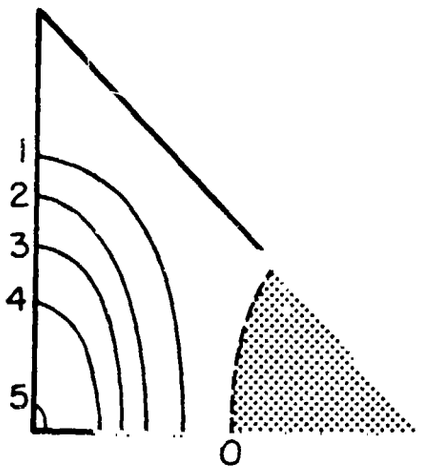
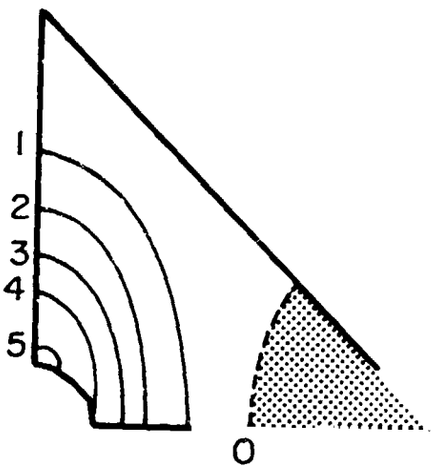


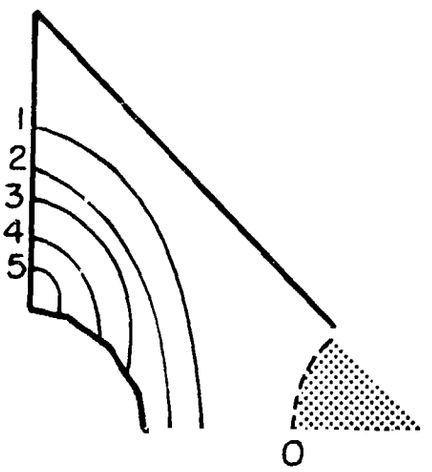
FIGURE 12 - Pre-buckling In-plane Stiffness as Function of Various d/b Ratios. Unstiffened Plates.



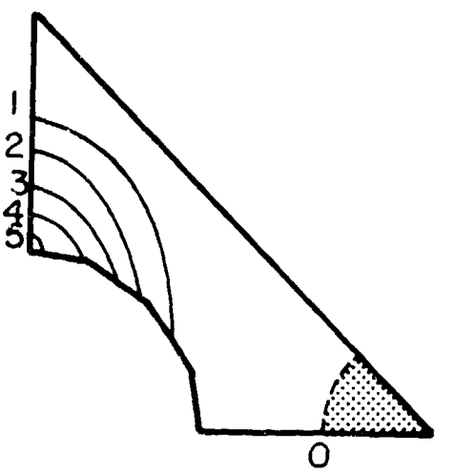
a. Unperforated



b. d/b = 0.2



c. d/b = 0.4



d. d/b = 0.6

FIGURE 13 - Contour Plots of Normal Modal Displacements for Various d/b Ratios.

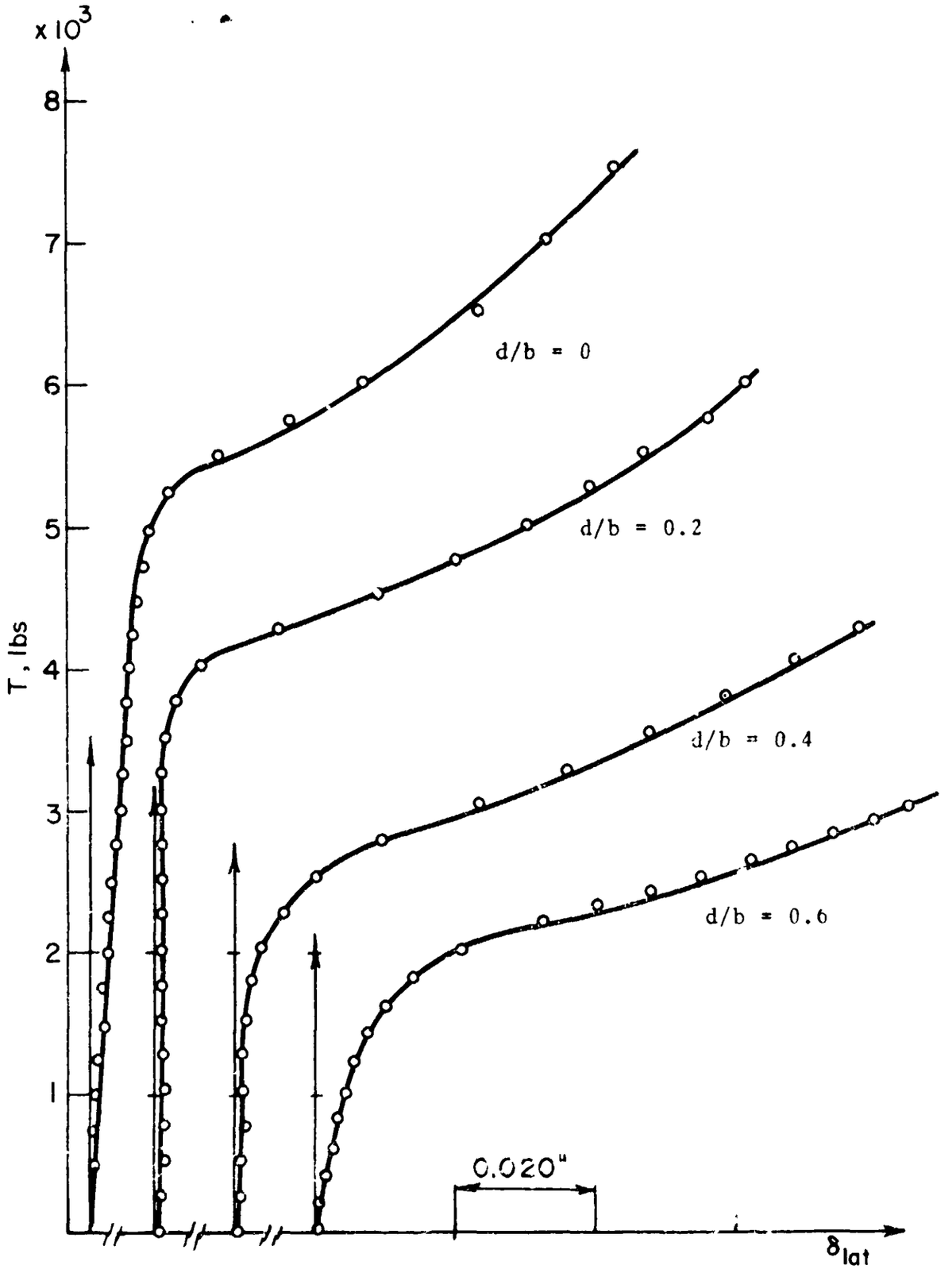
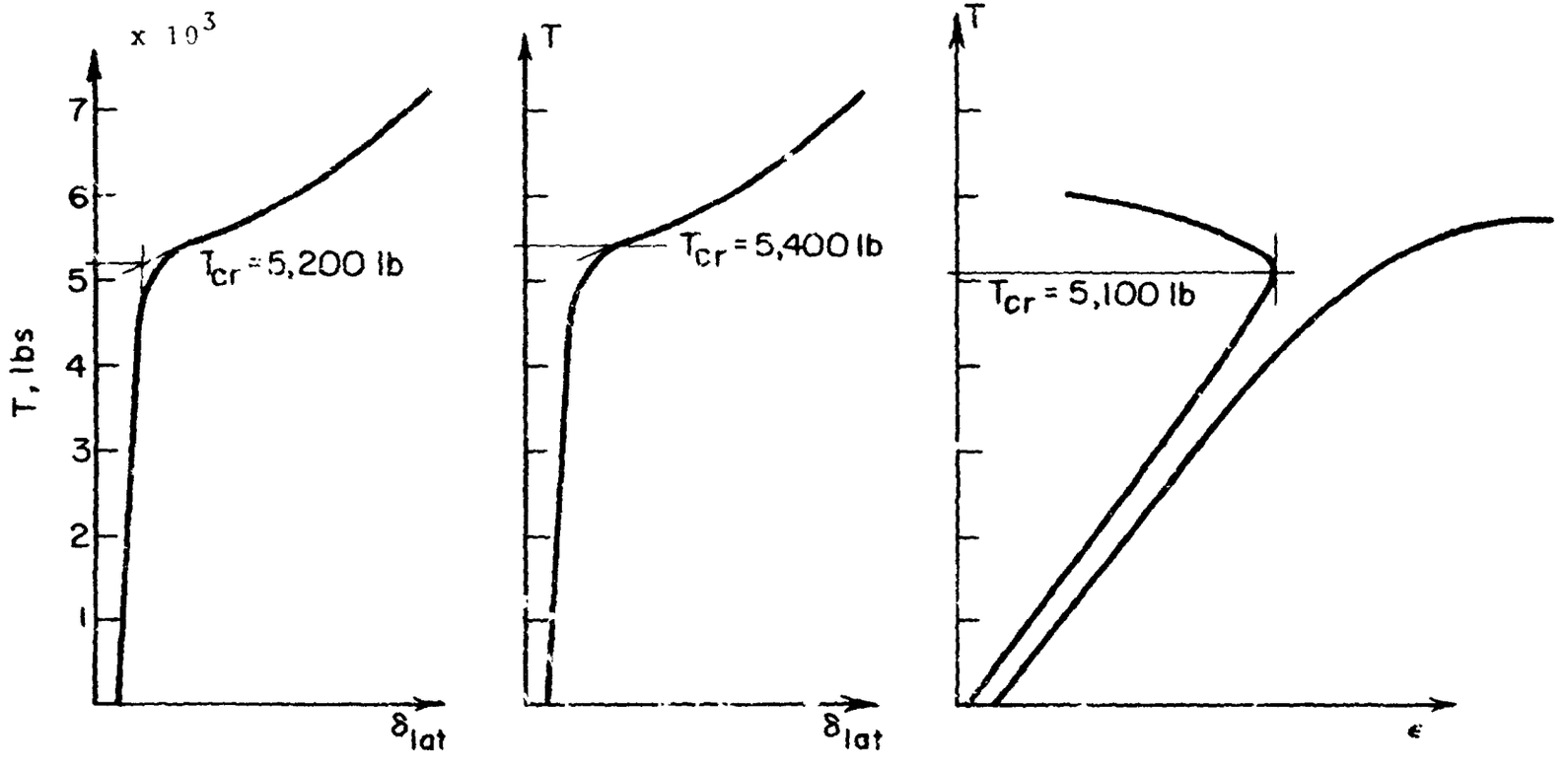


FIGURE 14 - T vs. δ_{lat} for Four Unstiffened Plates



a. Slope Interaction Method

b. Inflection Point

c. Strain Reversal

FIGURE 15 - Criteria for Defining Critical Buckling Load Applied to Test Data for Unperforated Plate.

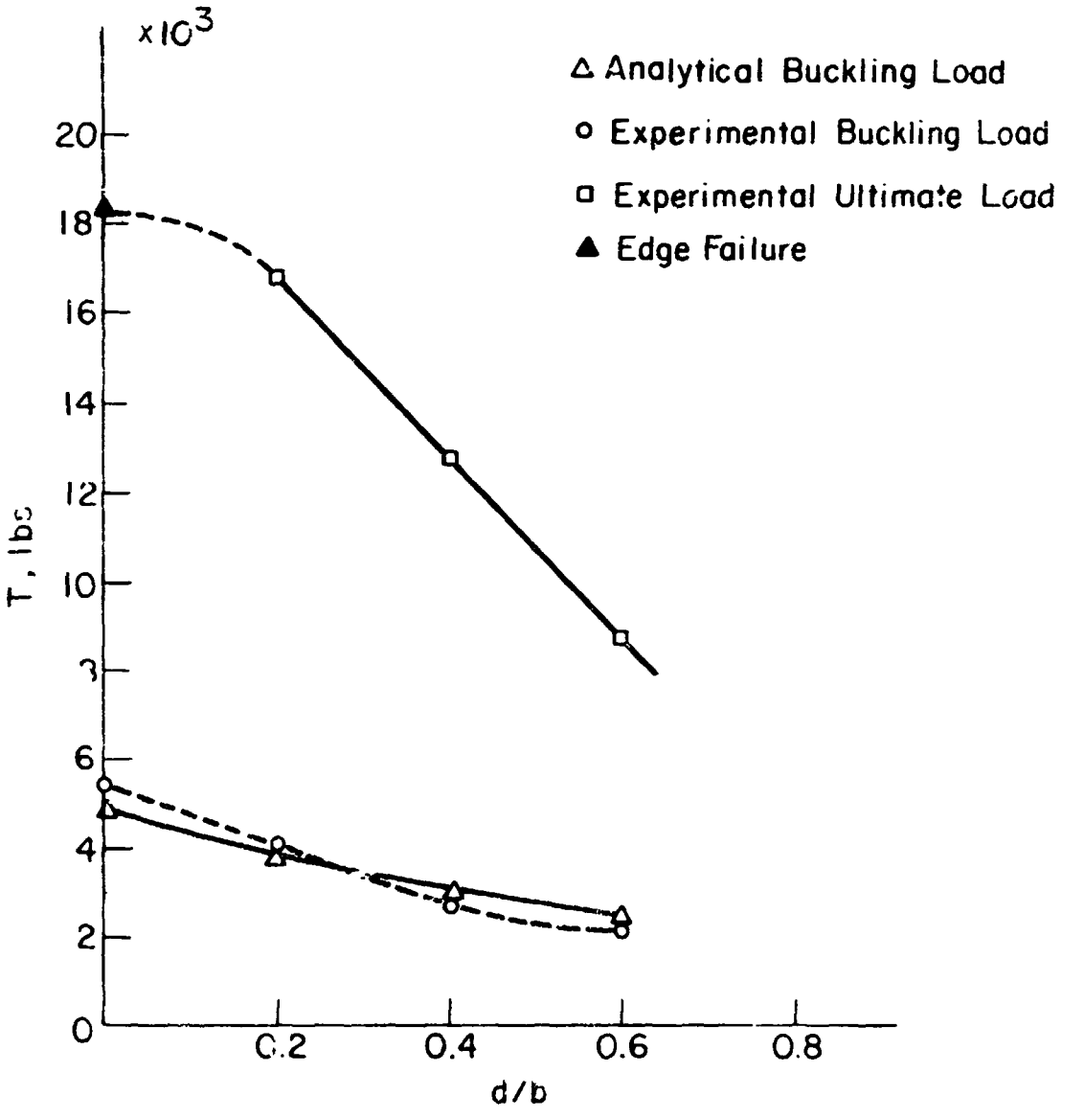
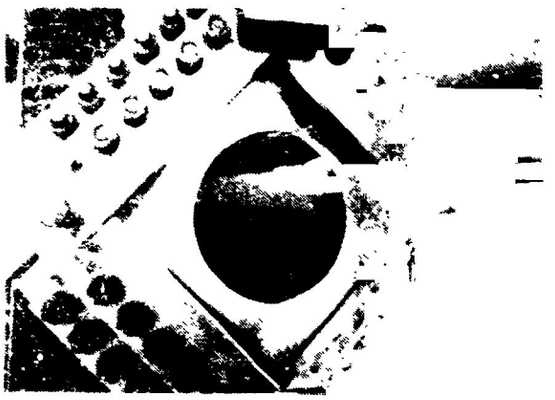
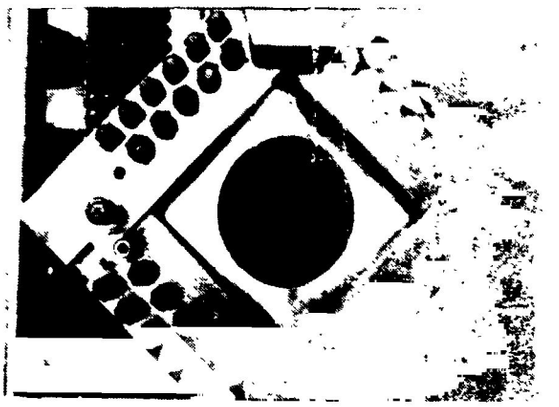


FIGURE 16 - Buckling and Ultimate Loads Determined from Test Results for Various d/b Ratios.

REPRODUCIBILITY OF THE ORIGINAL PAGE IS POOR.



a. Initial Buckling



b. Post-Buckling



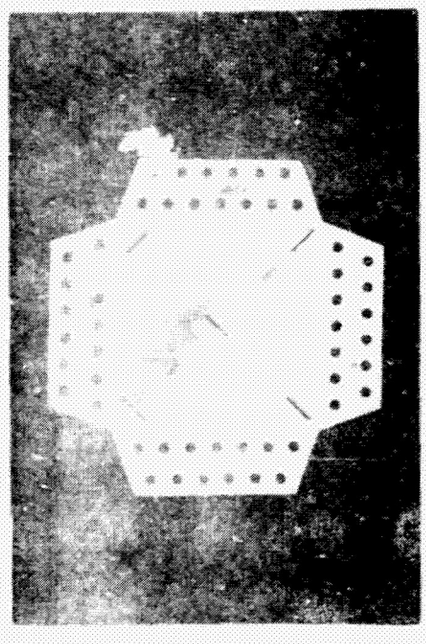
c. Vertical Crease Appears - Permanent Deformation



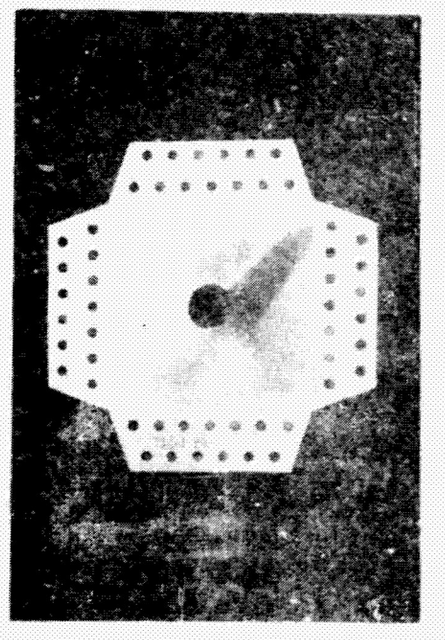
d. Failure at Edge of Plate

Fig. 17 - Post-Buckling Behavior of Plate with Uniform Edge Shear Deformation with d/b = 0.6.

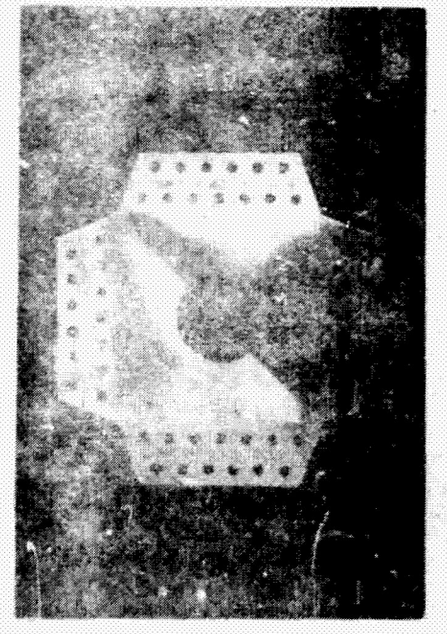
REPRODUCIBILITY OF THE ORIGINAL PAGE IS POOR.



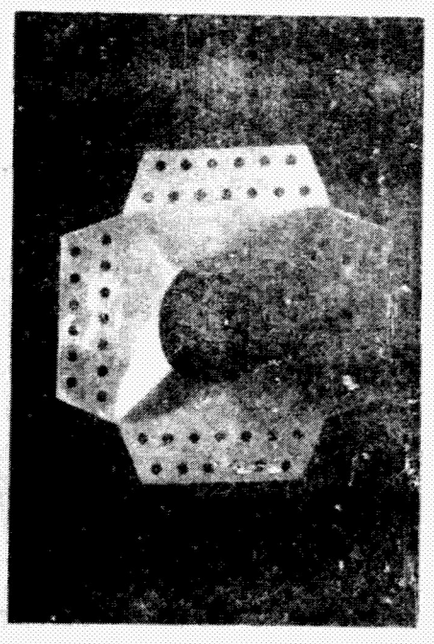
a. Unperforated (d/b = 0)



b. d/b = 0.2



c. d/b = 0.4



d. d/b = 0.6

FIGURE 18 - Specimens After Testing

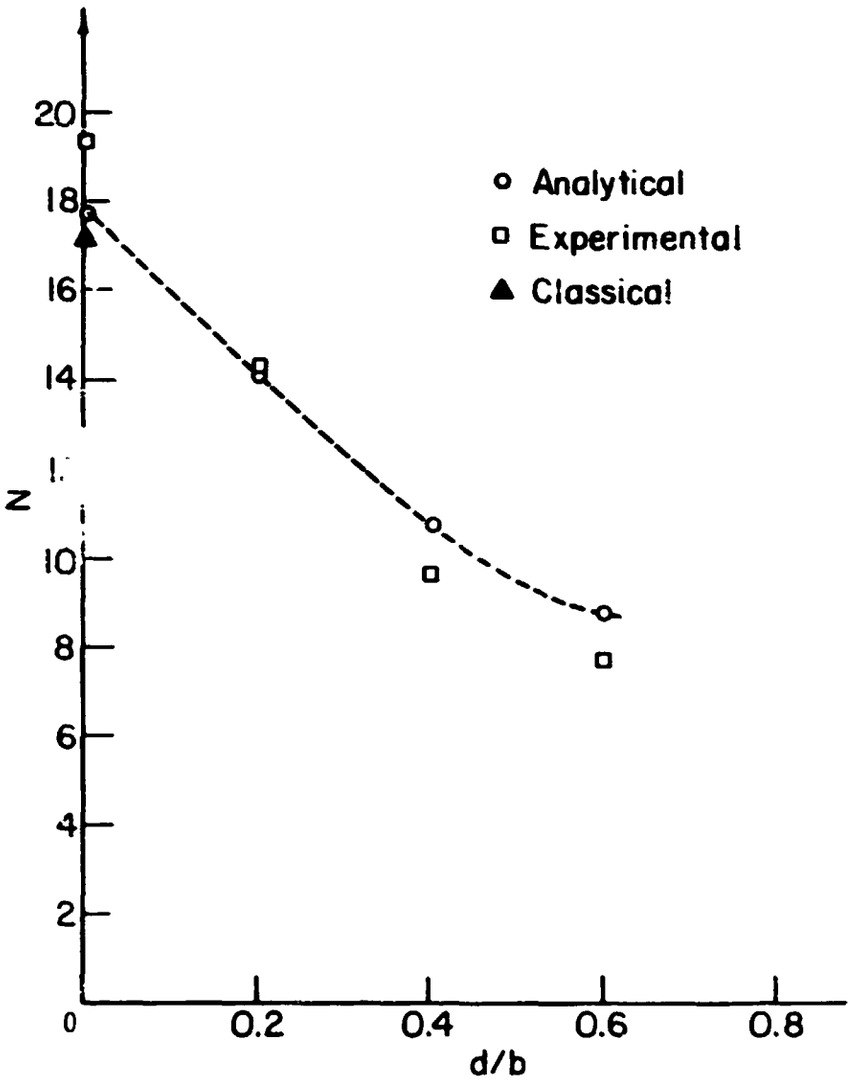


FIGURE 19 - Comparison of Experimental and Analytical Buckling Loads for Various d/b Ratio.

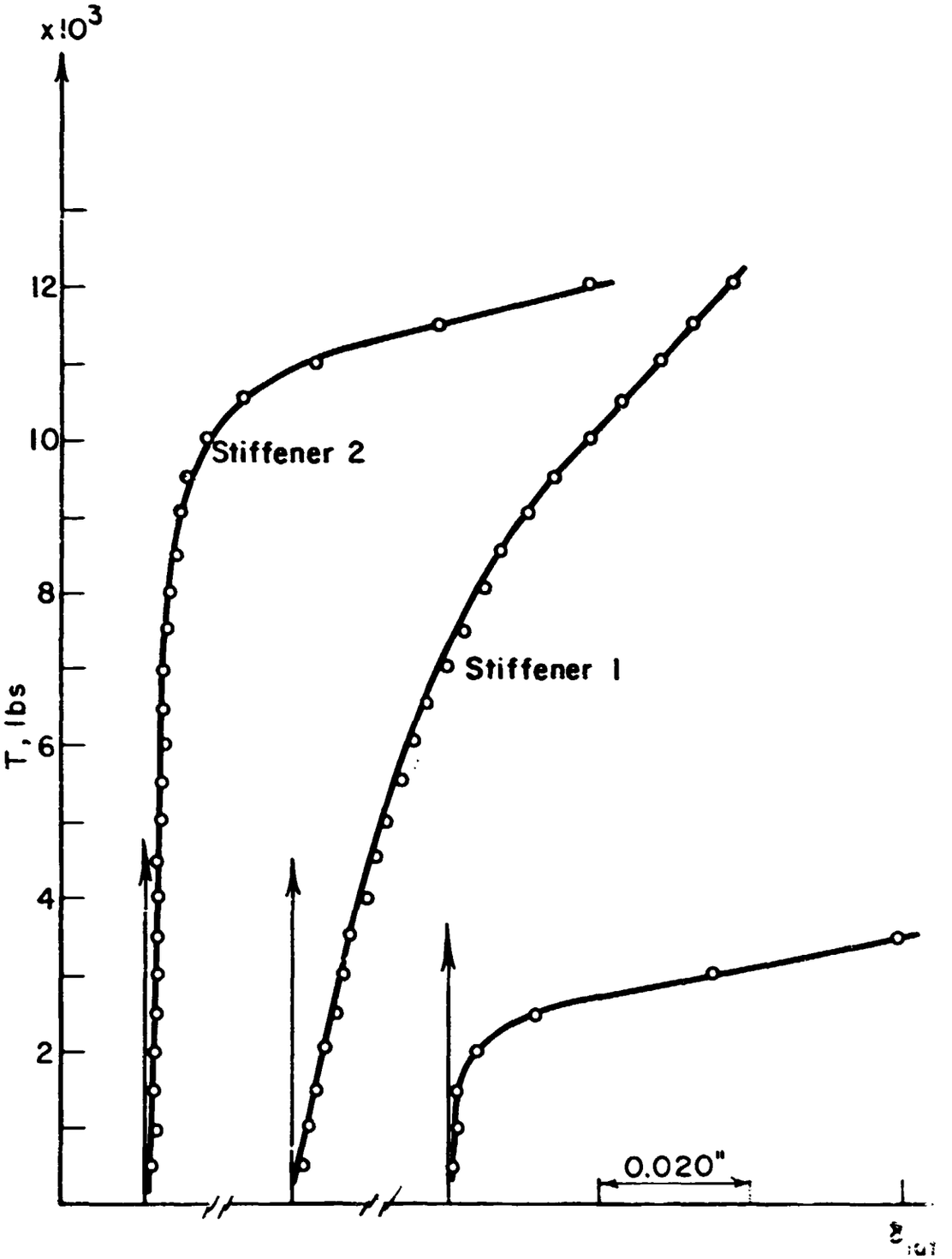


FIGURE 20 - T vs. δ_{lat} for Equal Cross-section Stiffeners

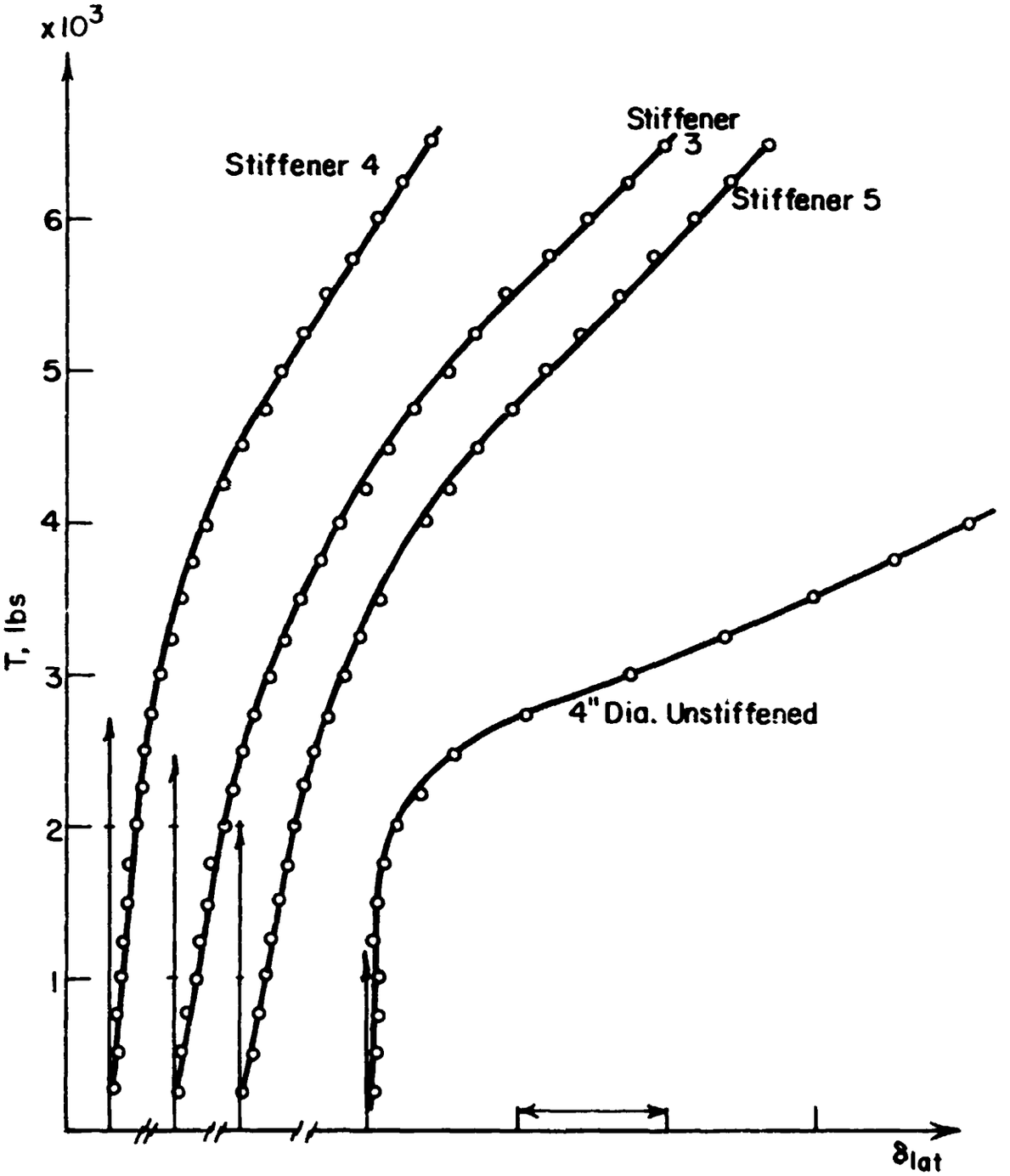


FIGURE 21 - T vs. δ_{lat} for Equal Volume Stiffeners

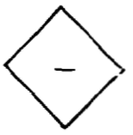
d/b	STRAIN LOCATION	T, lb.	STRAIN	
			ANALYSIS	EXPERIMENT
.0		2,500	376×10^{-6}	350×10^{-6}
.2		2,000	278×10^{-6}	319×10^{-6}
.4		1,500	354×10^{-6}	462×10^{-6}
.6		1,200	473×10^{-6}	531×10^{-6}

TABLE 1 - Comparison of Analysis and Test Strains at Selected Gage Locations.

d/b	STIFFENER	T_{cr}, lb. (EXPER.)
0	NONE	5,400
.4	NONE	2,700
.4	#1	9,100
.4	#2	11,300
.4	#3	5,000
.4	#4	4,800
.4	#5	4,500

TABLE 2 - Inflection Point Buckling Loads for Both Unperforated Plate and Stiffened and Unstiffened Plates with 4-Inch Perforation.